Bio-Design and Manufacturing (2022) 5:497–511
https://doi.org/10.1007/s42242-022-00196-1

RESEARCH ARTICLE

3D printing of osteocytic Dll4 integrated with PCL for cell fate determination towards osteoblasts in vitro

Pengtao Wang[1] · Xiaofang Wang[1] · Bo Wang[1] · Xian Li[2] · Zhengsong Xie[1] · Jie Chen[1] · Tasuku Honjo[3] · Xiaolin Tu[1]

Received: 17 November 2021 / Accepted: 3 March 2022 / Published online: 18 April 2022

Abstract

Since 3D printed hard materials could match the shape of bone, cell survival and fate determination towards osteoblasts in such materials have become a popular research target. In this study, a scaffold of hard material for 3D fabrication was designed to regulate developmental signal (Notch) transduction guiding osteoblast differentiation. We established a polycaprolactone (PCL) and cell-integrated 3D printing system (PCI3D) to reciprocally print the beams of PCL and cell-laden hydrogel for a module. This PCI3D module holds good cell viability of over 87%, whereas cells show about sixfold proliferation in a 7-day culture. The osteocytic MLO-Y4 was engineered to overexpress Notch ligand Dll4, making up 25% after mixing with 75% stromal cells in the PCI3D module. Osteocytic Dll4, unlike other delta-like family members such as Dll1 or Dll3, promotes osteoblast differentiation and the mineralization of primary mouse and a cell line of bone marrow stromal cells when cultured in a PCI3D module for up to 28 days. Mechanistically, osteocytic Dll4 could not promote osteogenic differentiation of the primary bone marrow stromal cells (BMSCs) after conditional deletion of the Notch transcription factor RBPjκ by Cre recombinase. These data indicate that osteocytic Dll4 activates RBPjκ-dependent canonical Notch signaling in BMSCs for their oriented differentiation towards osteoblasts. Additionally, osteocytic Dll4 holds a great potential for angiogenesis in human umbilical vein endothelial cells within modules. Our study reveals that osteocytic Dll4 could be the osteogenic niche determining cell fate towards osteoblasts. This will open a new avenue to overcome the current limitation of poor cell viability and low bioactivity of traditional orthopedic implants.

Graphic abstract

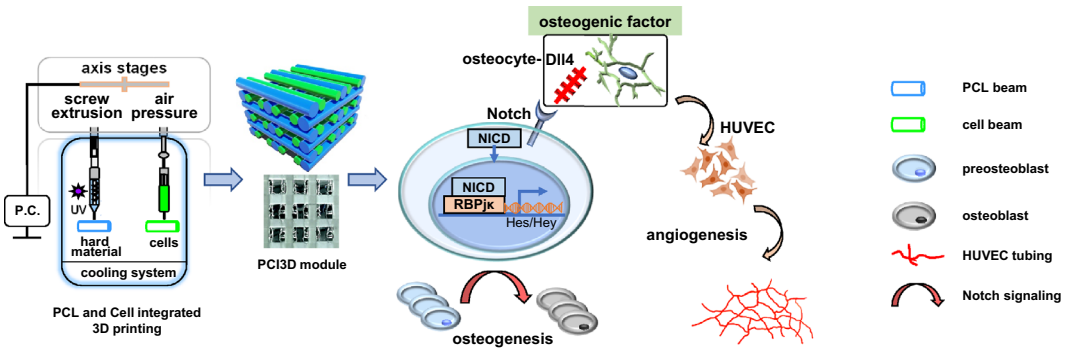

Pengtao Wang, Xiaofang Wang, Bo Wang and Xian Li have contributed equally to this work.

✉ Xiaolin Tu
xtu@cqmu.edu.cn

1 Laboratory of Skeletal Development and Regeneration, Institute of Life Sciences, Chongqing Medical University, Chongqing 400016, China

2 Medical Data Science Academy, Chongqing Medical University, Chongqing 400016, China

3 Department of Immunology and Genomic Medicine, Graduate School of Medicine, Kyoto University, Yoshida Konoe-cho, Sakyo-ku, Kyoto 606-8501, Japan

Keywords Integrated 3D printing · PCL scaffold · Cell-laden hydrogel · Osteocytic Dll4 · Bone marrow stromal cell · Osteoblast differentiation · Cell viability in hard material · RBPjκ · Notch signaling

Introduction

Bone is the second common transplantation tissue in the world. More than 4 million patients with bone defects use bone grafts or substitutes for surgical repair and treatment each year [1]. The increasing medical burden of bone diseases promotes the development of effective strategies for bone regenerative therapy [2]. Orthopedic implants need to be generally renovated within 5–20 years mainly due to the difficulty of matching individual shape and insufficient biological activity, while the renovation task is a great challenge for physicians. In addition, the healing process for the elderly or osteoporosis patients after skeletal fracture is slow. These issues are complicated to solve with the currently used materials. Hence, advanced research is urgently needed to restore bone structural integrity and enhance the osteogenic potential for tremendous unmet clinical needs.

Modern bone tissue engineering (BTE) strategies, including the reconstruction of three-dimensional (3D) scaffolds, have been developed to create "osteogenic" substitutes to repair bone diseases or defects [3, 4]. In addition, as bone is a supporting but functional organ, it is necessary to reconstruct 3D scaffolds possessing mechanical support together with a suitable microenvironment for bone cells to fulfill their biological functions. In other words, guiding osteoblast differentiation on hard scaffolding materials should be a central focus of modern BTE. Therefore, bioprinting cell-filled hydrogels with weak mechanical support is only the basis for advancing BTE. Decellularized extracellular matrix on hard scaffolds could also be another approach to provide the intrinsic environments for bone cells that is conducive to guiding the differentiation towards osteoblasts.

Fortunately, a milestone was reached in the progress of BTE in 2016: a novel 3D bioprinting system—the integrated tissue and organ printer (ITOP) [5]—could reconstruct polycaprolactone (PCL) and human amniotic fluid stem cells-encapsulated hydrogel as a novel 3D module. When this is implanted into the parietal bone of mice after 14 days of culture in vitro, the transplants develop into vascularized bone. This technique represents the direction of future 3D printing, which is applicable to clinics [6, 7]. Nevertheless, the generation of whole organs still has a long way to go possibly due to lack of cell fate guidance. Later, other teams successively applied this 3D printing technology with the integration of bioactive ions [8] or stem cells with human umbilical vein endothelial cells (HUVECs) [9], promoting osteogenic differentiation and vascularization. However, osteogenesis occurs naturally without defined molecular mechanisms, and it is still a huge challenge to discover and create osteogenic microenvironments that can be controlled at will.

The 3D bioprinting of hard scaffold materials combined with cell-loaded biological ink or bioactive factors constitutes a promising alternative path. This not only includes the fabrication of structures with physiological function to eliminate the limitations of traditional grafts, but also has great potential for bone regeneration. At present, there are still few cells that can grow deep inside a hard material [10]. Therefore, finding intrinsic environments with unique molecules or developmental signals to induce cell adhesion and proliferation has become the primary consideration in modern BTE, in order to incorporate a physiological and strict function orientating osteogenesis. In other words, it is of great significance to develop bioactive 3D scaffolds to integrate cell signal events for cell fate determination [11].

Three-dimensional scaffolds not only provide structural support for cells to adhere to and proliferate, but also serve as morphogenetic agents to guide cell differentiation, tissue regeneration, and tissue structure maintenance [12–14]. However, at present, such attempts are still limited by the uncertainty and controversy around cell source and active molecule selection [15, 16]. Bone marrow stromal cells (BMSCs) have the potential to develop bone-forming osteoblasts, making them a valuable cell source for BTE [17, 18]. Meanwhile, osteocytes could be a more ideal cell source for BTE due to their intrinsic bone environment for regenerative rehabilitation and their highest abundancy of more than 90% of total bone cells [19, 20]. Although embedded in the bone matrix, osteocytes were found to be the active mediator for bone remodeling and formation in our generated mouse models, featuring the activation of β-catenin signaling in osteocytes [21]. Osteocytic Wnt is sufficient to generate the components of the Notch signaling pathway, including Notch signal-sending molecules Jag1, Jag2, and Dll4. Notch signaling plays an important role in bone development and remodeling. The receptors Notch 1 to 4 directly interact with the ligands of the jagged-like (Jag1, Jag2) and delta-like (Dll1, Dll3, Dll4) families, followed by the activation of Notch signaling to induce the transcription of Notch target genes [22–24].

In this study, we established a new PCL and cell-integrated printing system (PCI3D) to interactively manufacture PCL beams and cell beams as cell-laden hydrogels for reconstructing functional 3D modules. To solve the bottleneck problem of cell survival and growth on hard materials, PCI3D modules provide a stable supporting scaffold with suitably sized apertures, which enables the easy transport and discharge of materials necessary for cell growth, their differentiation to osteoblasts, and mineralization. Osteocytes overexpressing the Notch ligand Dll4 act as an independent osteogenic

factor in the cell-encapsulated hydrogel to promote either primary or cell line of mouse BMSCs via the RBPjκ-dependent canonical Notch signaling pathway. We further identified that in osteocytes on hard scaffolding biomaterial, only Dll4 of the Notch ligand delta-like family, but not Dll1 or Dll3, greatly promotes osteogenesis with a potential function of angiogenesis. This study reveals that the design of mechanical scaffolds integrated with cellular events may be a promising strategy for BTE for the regenerative repair of bone defects.

Materials and methods

Animals

The RBPjκ$^{f/f}$ mouse strain, in which the Notch signaling transcription factor RBPjκ is genetically modified with Cre recombinase-recognized codes, was kindly provided by Dr. Tasuku Honjo [25]. All processes were performed in accordance with the guidelines of the Experimental Animal Center of Chongqing Medical University.

Cell culture

The culture of murine primary and cell line (ST2) of BMSCs was performed as previously reported [26]. The osteocytic cell line MLO-Y4 was kindly provided by Professor Lynda Bonewald [27]. HUVECs were purchased from the American Type Culture Collection (ATCC; Manassas, VA, USA). The cells were cultured in α-MEM medium (Gibco, USA) containing 10% fetal bovine serum (FBS, BI, Israel) with 50 U/mL penicillin and 50 μg/mL streptomycin (Beyotime, China) at 37 °C under 5% CO_2. Half of the medium was replaced once every 2–3 days. The BMSCs were passed once at day 7 or 8 after seeding, and reseeded at a density of 1.5 × 10^5 cells/cm^2 for osteoblast differentiation assays. The MLO-Y4 and ST2 cells were placed in each well of 24-well plates at a density of 2 × 10^4 and 8 × 10^4 cells, respectively, and co-cultured for 3 days.

Stable transfection of MLO-Y4 with lentivirus

Lentiviruses containing Dll1, Dll3, or Dll4 genes were individually transfected into MLO-Y4 cells at a multiplicity of infection (MOI) of 100 with 7 μg/mL polybrene (Sigma, USA). The efficiency of each lentiviral infection cycle was determined by the intensity of GFP fluorescence after 72 h of culture. The cells were then selected using a medium containing 0.5 μg/mL puromycin (MCE, USA) for more than one week to eliminate cells without lentiviral vectors.

Deletion of RBPjκ in BMSCs

The two recombinant adenoviruses Ad-Cre and Ad-GFP were constructed by the Ad-Easy system (GENE, China) and amplified in 293HEK cells. The titer of the viruses was quantified in BMSCs from RBPjκ$^{f/f}$ mice to remove the RBPjκ ex vivo.

Integration of biomaterials and cells into 3D printing

Lyophilized Gelatin Methacryloyl (GelMA, Sunp biotech, China) was fully dissolved in α-MEM media to create a 20% (w/v) GelMA solution containing 0.5% (w/v) photo-crosslinking agent (LAP, Sunp biotech, China), that was sterilized through a filter (0.22-μm, Merck Millipore, Darmstadt, Germany) as stocking solution, and stored at 4 °C until further use. The mixing ratio of 1:4 had been previously tested to produce the best osteogenic differentiation effect. The cell suspension was measured as 2 × 10^5 MLO-Y4 cells and 8 × 10^5 ST2 or HUVEC, which were suspended in 0.5 mL α-MEM. After mixing with an equal volume of cell suspension, the final concentration of GelMA was set as 10% (w/v) and LAP was 0.25% (w/v). Subsequently, the cell-loaded solution was placed into a syringe and refrigerated on ice, and then the cooled syringe was put in the cell-printing nozzle (ALPHA-IPT1, Sunp Biotech, China), ready for printing.

Next, the biomaterial polycaprolactone (PCL, Sigma, USA) was loaded into the hard material nozzle and melted in advance for 30 min at 95 °C, which temperature was found as the best temperature for PCL printing in this study. In particular, the melted PCL was extruded out as beams in a diameter of 400 μm with an interval of 1100 μm between PCL beams at a speed of 2 mm/s. The cell-loaded GelMA solution was reciprocally printed out at 25 °C as cell beams in a diameter of 300 μm with an interval of 500 μm between cell beams at a printing speed of 5 mm/s [28]. After the printing of one layer, the GelMA hydrogels were crosslinked under blue light at 405 nm for 10 s, and the PCL and solidified cell beams were reconstructed to form a single layer.

Then, printing was continued for another layer, in which the printed PCL beams and cell beams were perpendicular to the ones of the neighboring layer. After three layers of printing, a PCL and cell-integrated 3D (PCI3D) module was fabricated. The PCI3D modules were placed in the complete cell growth medium in a 6-well plate and cultured in an incubator at 37 °C under 5% CO_2 for subsequent experiments.

In our dual nozzle printing system, the melting PCL is extruded out by a screw propeller with elevated pressure to drive out the hard material, and the cell beams, encapsulated by hydrogel, are extruded out by air pressure.

Table 1 Sequences of primers used for qRT-PCR

Primer	Forward	Reverse
GAPDH	GCACATCAAGGCCGAGAAT	GCCTTCTCCATGGTGGTGAA
Dll1	CTGTGCTGCTGTGGTGGTCTG	AGTCCGCCTTCTTGTTGGTGTTC
Dll3	CGCCGCACTCTTGGTCATCC	CCAGCACCGTCTTGTAACCTCAG
Dll4	TACCTTGACCTGCGCGGACTC	TCGGCTTGGACCTCTGTTCTGG
Alp	CACGGCGTCCATGAGCAGAAC	CAGGCACAGTGGTCAAGGTTGG
Runx2	CCGGTCTCCTTCCAGGAT	GGGAACTGCTGTGGCTTC
Osx	CCCTTCTCAAGCACCAATGG	AAGGGTGGGTAGTCATTTGCATA
Col1	GACAGGCGAACAAGGTGACAGAG	CAGGAGAACCAGGAGAACCAGGAG
Hey1	CACTGCAGGAGGGAAAGGTTAT	CCCCAAACTCCGATAGTCCAT
Hey2	CAGCTGCACACAGCTTCC	CTGCGGATACCGACAAGG
Hes1	TACCCCAGCCAGTGTCAACA	TCCATGATAGGCTTTGATGACTTTC
Hes7	GATGCTGAAGCCGTTGGTGGAG	TCCAGGAGCAGCAGCCTCAG
Hes5	TGCAGGAGGCGGTACAGTTC	GCTGGAAGTGGTAAAGCAGCTT
Vegfa	AGAAGGAGGAGGGCAGAATCATCAC	GGGCACACAGGATGGCTTGAAG
Hif1α	CCATTAGAAAGCAGTTCCGCAAGC	GTGGTAGTGGTGGCATTAGCAGTAG
eNOS	TCACCTTCTTCCTGGACATCACTC	ACCACTTCCACTCCTCGTAGCG
VE-Cad	TGCCTCCTATCCCAGTGTCGTATC	GCCTCGGTTCCCATATCTCATCTTG

Cell viability assay

The viability of cells in PCI3D modules was quantified by the LIVE/DEAD™ Cell-Mediated Cytotoxicity Kit (Thermo Fisher, USA). After 1 day of cell culture, the medium was replaced by the staining mixture, which was prepared by mixing 0.5 μL Calcein-AM (0.5 μL/mL) with 2 μL ethidium homodimer-1 (EthD-1, 2 uL/mL) in phosphate buffered saline (PBS). The plates were incubated at 37 °C for 1 h, thoroughly washed 3 times with PBS, and immediately imaged using an inverted fluorescence microscope (LEICA, Germany). The cell viability was quantified using ImageJ software (Fiji ImageJ).

Cell proliferative activity

The Cell Counting Kit-8 (CCK-8, Beyotime, China) was used to evaluate the proliferation activity of cells in the functional modules at day 1, 4, and 7 step by step. For this assay, modules were washed with PBS, divided into 4 pieces, and placed in a 96-well plate. Next, 90 μL PBS and 10 μL CCK-8 solution were added to each well followed by 2-h incubation. Subsequently, the supernatant was pipetted into a new 96-well plate, and the absorbance was measured at 450 nm using a microplate reader.

RNA extraction and gene expression analysis

The total RNA of cells was extracted using the TRIzol reagent (Invitrogen, USA), and cDNA was synthesized from the total RNA extraction through a reverse transcription reaction kit (TAKARA, Japan). The synthesized cDNA was diluted five-fold prior to storage until use as templates for quantitative real-time polymerase chain reaction (qPCR) to detect genes with primer sets (Table 1). The relative expression levels of mRNAs were normalized to the housekeeping gene GAPDH by using the $2^{-\Delta CT}$ method.

Alkaline phosphatase staining

Cells or PCI3D modules were washed with PBS (Sorlabio, China) after culture for the indicated number of days, and then fixed with 3.7% formaldehyde (Chuandong, China) for 5 min at room temperature. According to the instruction of BCIP/NBT alkaline phosphatase (AP) color development kit (Beyotime, China), the dye solution was added to the culture plate to stain for 30 min or 4 h for the cells in monolayer culture on plates or 3D culture in the modules, respectively, in a dark box at room temperature. The staining of cells was recorded by a regular digital camera.

AP biochemical activity assay

The AP biochemical activity assay was performed as previously described [26]. Briefly, 0.3 mL 10 mM Tris/HCl (pH 7.4) was added to each well, the cells were removed from the plate by scratching, and then sonicated on ice. After centrifugation at full speed, the supernatant was used for assay with an AP detection kit step-by-step as per the described procedures (Beyotime, China).

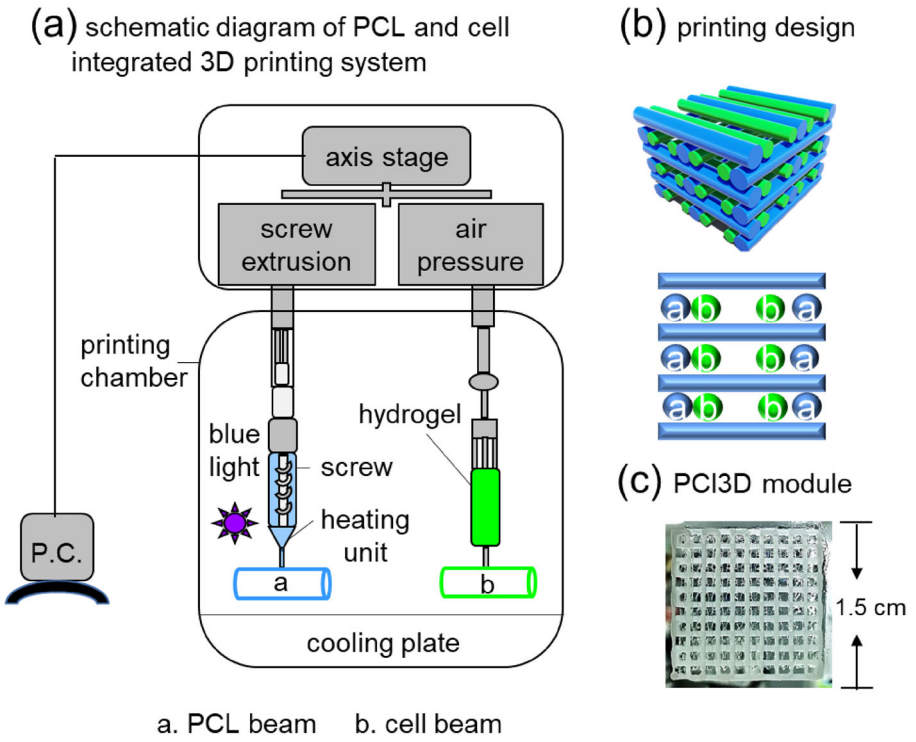

Fig. 1 3D printing of a PCL and cell-integrated functional module. **a** Schematic diagram of PCL and cell-integrated 3D printer. **b** Layout of cross section of PCL and cell beams in the printed functional module. **c** Image of a printed functional module. PCL, polycaprolactone; P.C., personal computer; PCI3D, a PCL and cell-integrated 3Dprintingsystem; a, PCL beam; b, cell beam

Matrix mineralization assay (Alizarin Red S staining)

The PCI3D modules were cultured in the growth medium for 7 days, and bone nodule formation was induced in the osteogenic medium containing 0.1 mM dexamethasone, 10 mM β-glycerophosphate disodium salt solution, and 50 μg/mL L-ascorbic acid for 14 days. Matrix mineralization was analyzed by Alizarin Red S staining [26]. The modules were stained with 0.4% Alizarin Red S for 30 min, and then pictures were taken. Subsequently, the modules were extensively washed with PBS at room temperature, the stained bone nozzles were destained in 10% cetylpyridinium chloride for 1 h, and the washing solution was collected for absorbance measurement at 562 nm to quantify the mineralization status [29].

In vitro HUVEC tube formation assay

Human umbilical vein endothelial cells (HUVECs) at 0.5×10^5 cells/cm^2 and MLO-Y4 at 1×10^4 cells/cm^2 were mixed and seeded onto pre-cooled 24-well plates containing 200 μL matrigel (Corning, USA) and cultured for 6 h at 37 °C under 5% CO_2 as previously reported [30]. Capillary-like structures were captured by a phase contrast microscope. The network structures formed from HUVEC cells were quantified by Image J.

Statistical analysis

All statistical analyses were performed by GraphPad Prism 8.0 software. Each experiment was repeated three times independently. The data were presented as mean ± SD. One-way ANOVA and two-way ANOVA were used to analyze the difference between multiple groups and two independent variables, respectively. Student's *t*-test was performed between two comparable groups, and $p < 0.05$ was considered as a significant difference.

Results

Reconstruction of PCL and cell-integrated 3D printing

A PCL and cell-integrated 3D printing (PCI3D) system was set up, consisting of two high-speed and precisely positioning nozzles with a temperature cooler. This system was equipped with two propellers using micro-mechanical extrusion and air pressure to alternatively produce beams of hard material and cell-loaded hydrogel in diameters of 400 and 300 μm, respectively. The hard material, such as PCL, was loaded into the heating cartridge and played the role of mechanical support, while the cells were loaded in hydrogel into the air-pressure syringe (Fig. 1a). As shown in the schematic diagram, the PCI3D system contains the uppermost *XYZ* axis

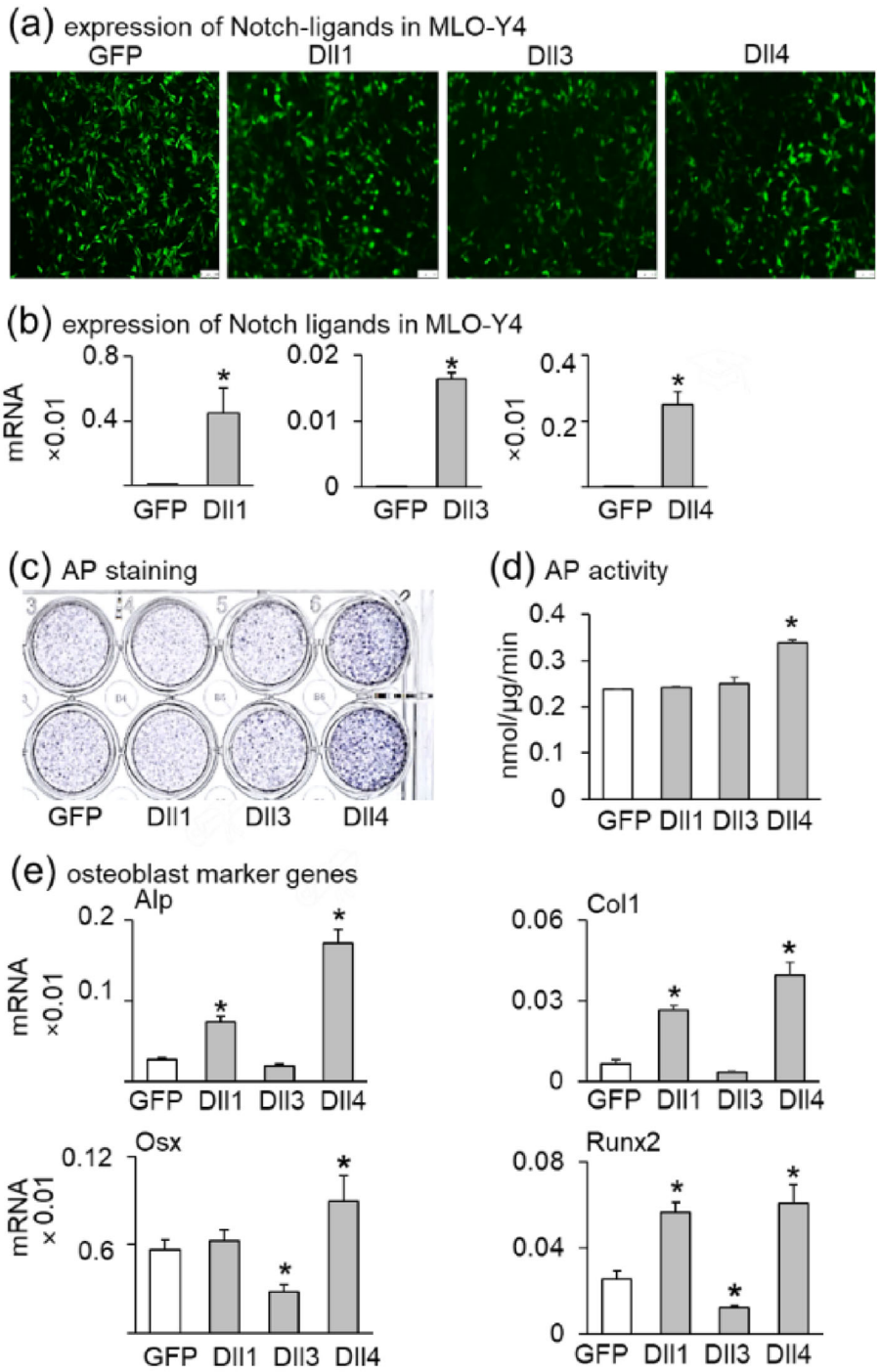

Fig. 2 Comparison of effect of osteocytic Dll1, Dll3, or Dll4 on osteoblast differentiation in the co-cultures with ST2 cells. **a** Selection of osteocytes infected with lentiviruses expressing Dll1, Dll3, Dll4, or its control GFP. Each Notch ligand co-expresses GFP as an indicator. **b** Gene expression in stably transfected osteocytes. **c, d** Osteoblast differentiation assays performed by AP staining (**c**), and its quantitative activity assay (**d**) in the co-cultures. **e** Expression of osteoblast marker genes in the co-cultures. GFP, Dll1, Dll3, or Dll4 represents GFP only, Dll1-, Dll3-, or Dll4-expressing MLO-Y4. $*p < 0.05$ versus GFP control by one-way ANOVA, $n = 3$. Scale bar = 100 μm

stage to print 3D structures by parallelly and reciprocally extruding beams of PCL and cells. The middle operating system is composed of a screw propeller in a heating unit for PCL and an air-pressure syringe for cells. The lowermost temperature-controlling plate is able to cool the printed module quickly. By repeated printing cycles, a functional PCI3D module was constructed (Figs. 1b and 1c). This module possesses stable support and tunnel-connection structure with a suitable aperture size for the transportation of nutrition and metabolic materials (Fig. 1c).

Comparison of osteoblast differentiation of osteocytic Dll1, Dll3, and Dll4 in ST2 cells

In order to investigate the effect of Notch ligands Dll1, Dll3 and Dll4 in osteocytes on osteoblast differentiation in ST2

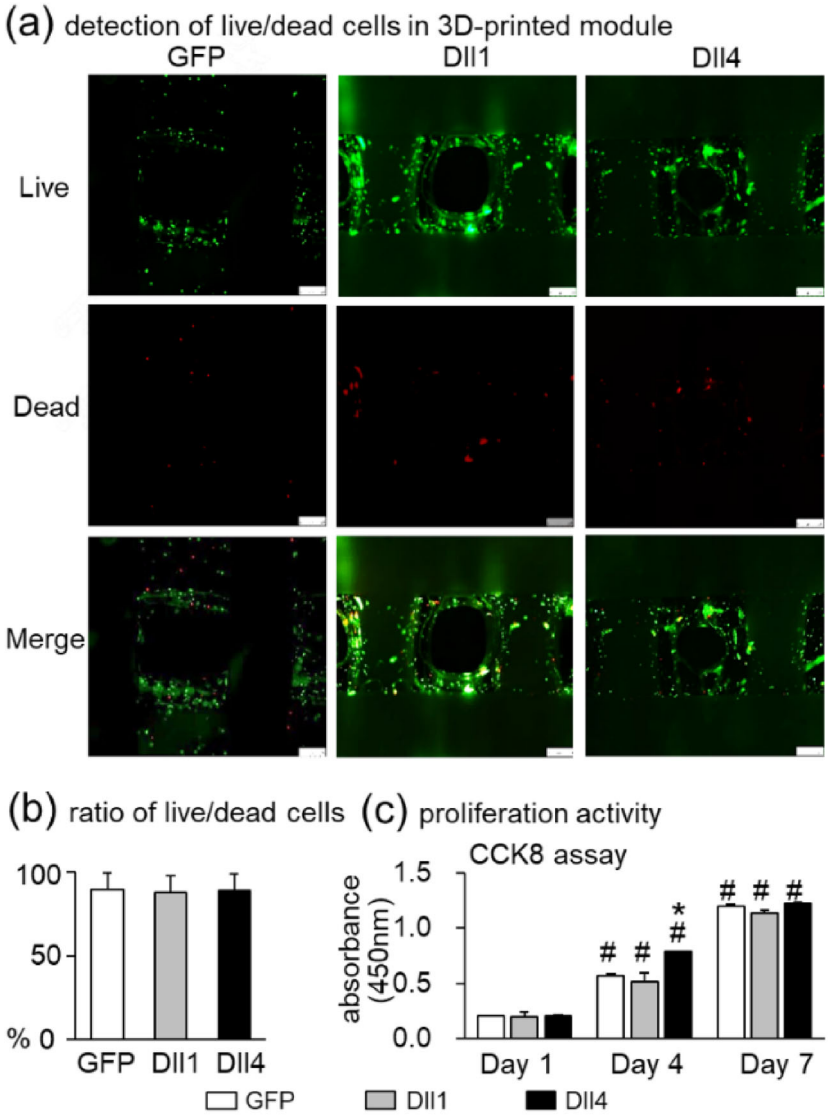

Fig. 3 Cell viability and proliferation activity in PCI3D modules. **a, b** Detection of live/dead cells (**a**) and its quantitative analysis (**b**) in the modules cultured for 1 day. **c** CCK8 assay for cell proliferation activity in modules. GFP, Dll1, or Dll4 represents GFP only, Dll1-, or Dll4-expressing MLO-Y4. $^{*}p < 0.05$ versus GFP; $^{\#}p < 0.05$ versus Day 1 by two-way ANOVA, $n = 3$. Scale bar = 100 μm

cells, the osteocytic cell line MLO-Y4 was infected with recombinant lentivirus carrying Dll1, Dll3 or Dll4 genes for 72 h. Puromycin was used to select MLO-Y4 cells with stable expressions of Dll1, Dll3, Dll4, or GFP (Fig. 2a). We generated MLO-Y4 cells overexpressing each Notch ligand together with GFP (MLO-Y4-Dll1, MLO-Y4-Dll3, and MLO-Y4-Dll4) or carrying GFP only as control (MLO-Y4-GFP). The qPCR assays showed that each of Dll1, Dll3, and Dll4 was expressed at a high level in each selected MLO-Y4 cell group compared to the MLO-Y4-GFP control (Fig. 2b).

The selected MLO-Y4 cells were co-cultured with ST2 cells at a ratio of 1:4 for 3 days. The AP staining and its biochemical activity assays indicated that the cells over-expressing Dll4, as opposed to Dll1 or Dll3 in MLO-Y4 cells, significantly promoted osteoblast differentiation in ST2 cells (Figs. 2c and 2d). Interestingly, both Dll1 and Dll4 in the co-cultured cells increased the expression of osteoblast marker genes, including Alp, Runx2, Col1, and Osx (Fig. 2e), suggesting a potential capacity of these two ligands for bone formation.

Comparison of cell viability and proliferation of osteocytic Dll1 and Dll4 in PCI3D modules

The PCI3D modules with MLO-Y4 cells overexpressing Notch ligand or GFP control and ST2 were cultured for 1 day, and live/dead cell assay was performed to detect cell viability. The live cells displayed Calcein-AM positive (green), and the dead cells were EthD-1 negative (red) (Figs. 3a and 3b). The results indicated high cell viability without significant differences among the functional modules of MLO-Y4-Dll1 at 87.74%, MLO-Y4-Dll4 at 89.23%, and MLO-Y4-GFP at 89.52%. The CCK8 assay on proliferation activity for 7 consecutive days showed that all of the cells in the PCI3D module

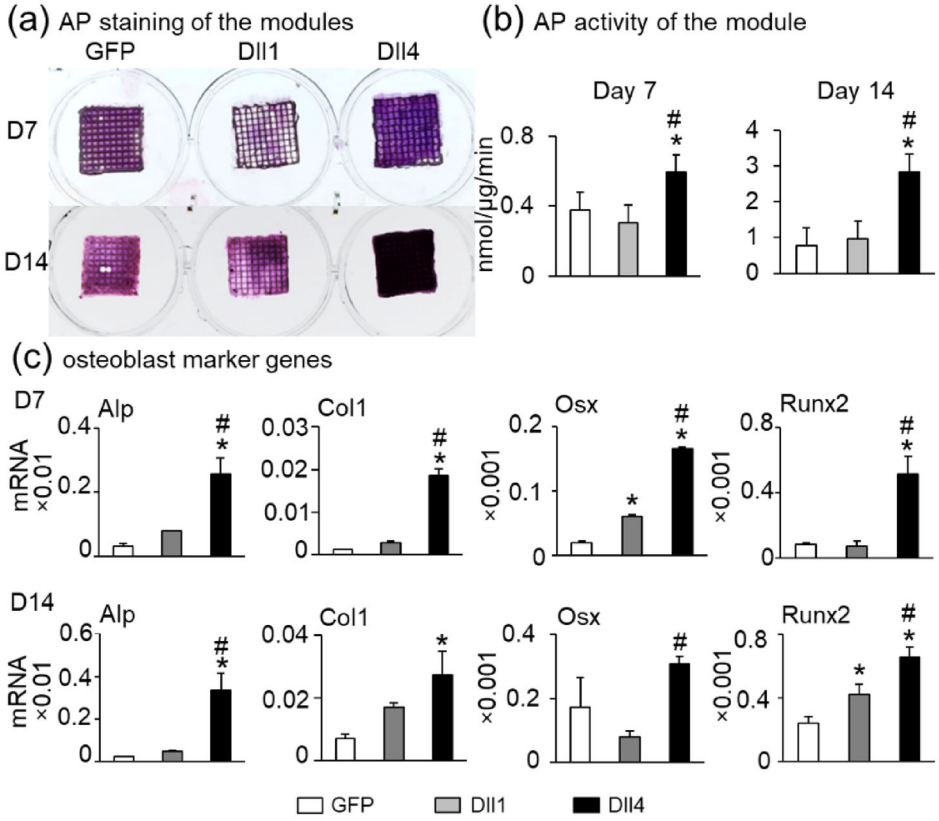

Fig. 4 Comparison of osteocytic Dll1 or Dll4 on osteoblast differentiation in PCI3D modules. **a–c** AP staining (**a**) and its biological activity assay (**b**), and gene expression of osteoblast markers (**c**) in the modules cultured for 7 or 14 days. GFP, Dll1, or Dll4 represents GFP only, Dll1-, or Dll4-expressing MLO-Y4. $^{*}p < 0.05$ versus GFP alone; $^{\#}p < 0.05$ versus Dll1 control by one-way ANOVA, $n = 3$. Scale bar = 100 μm

proliferated by nearly sixfold. However, Dll1 or Dll4 did not induce significant changes in proliferation activity compared to the GFP groups at day 7, although Dll4 displayed higher proliferation activity at day 4 (Fig. 3c). These results suggested that the PCI3D module provides a favorable environment for cell growth and proliferation.

Comparison of osteogenesis of osteocytic Dll1 and Dll4 in PCI3D modules

In order to further determine the effects of Dll1 and Dll4 on osteogenesis, the respective functional modules were cultured for 7 and 14 days and then subjected to AP activity assays. MLO-Y4-Dll4 significantly increased AP activity compared to the MLO-Y4-GFP and MLO-Y4-Dll1 groups (Figs. 4a and 4b), which was further confirmed by the qPCR results. Only the MLO-Y4-Dll4 group showed a significant increase in the expression of osteoblast marker genes Alp, Col1, Runx2, and Osx, as compared to the MLO-Y4-GFP or MLO-Y4-Dll1 group. Interestingly, unlike in two-dimensional (2D) culture (Fig. 2e), MLO-Y4-Dll1 did not enhance osteogenesis in the 3D modules. Thus, Notch ligand Dll4 in osteocytes induced osteoblast differentiation in ST2 cells.

Effect of osteocytic Dll1 and Dll4 on mineralization in the PCI3D modules

In order to evaluate the effects of Dll1 and Dll4 on bone nodule formation, PCI3D modules of MLO-Y4-GFP, MLO-Y4-Dll1, and MLO-Y4-Dll4 were cultured in vitro for 7 days in growth medium followed by 14 days in an osteogenic medium supplemented with ascorbic acid, β-glycerophosphate disodium, and dexamethasone. Alizarin Red S staining revealed stronger mineralization in Dll4 modules with larger and denser bone nodules formed (Figs. 5a and 5b), in which osteocytic Dll4 caused a twofold increase in calcium deposition compared to the MLO-Y4-GFP and MLO-Y4-Dll1 modules (Fig. 5c). Similar to the above assay, Dll1 had no significantly enhanced effect on mineralization compared to GFP control. Our results further confirmed the positive effect of Dll4 on osteogenesis in ST2 cells.

Osteogenic mechanism of osteocytic Dll4

Dll1, Dll3, and Dll4 are all ligands of the delta-like family in Notch signaling, but when overexpressed in osteocytes, they fulfill different roles in osteogenesis. Next, we examined the underlying mechanism by which cell fate can be determined

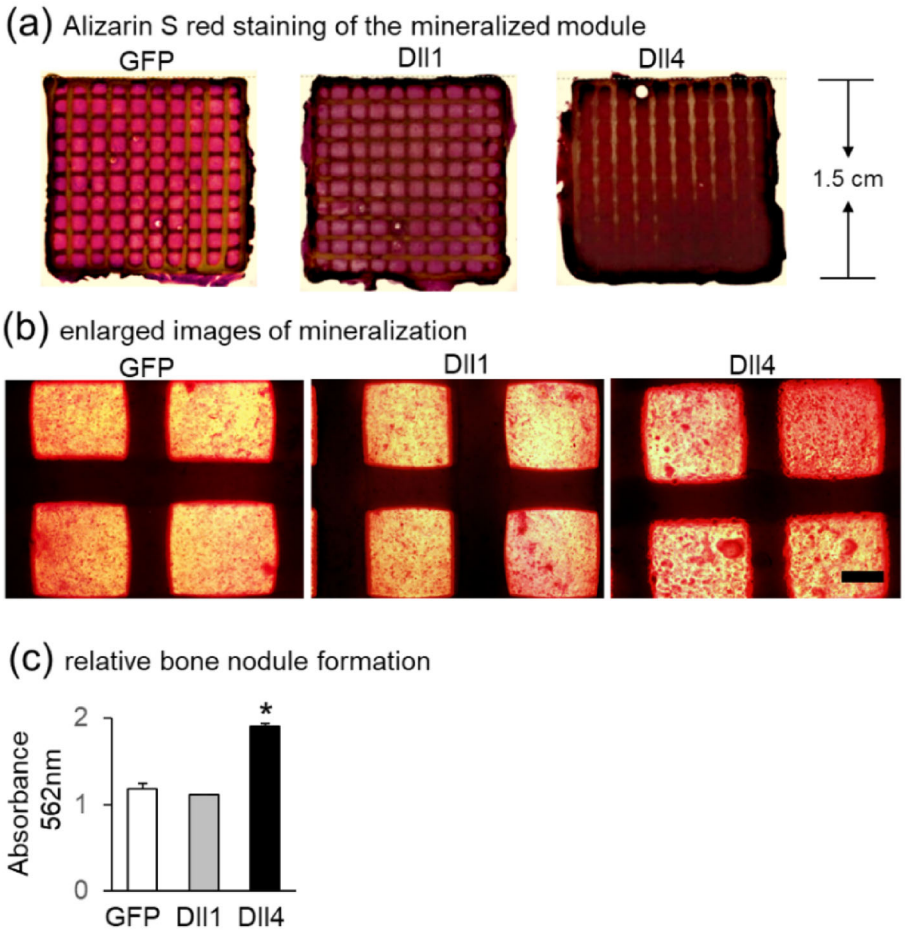

Fig. 5 Mineralization of induced osteoblasts in PCI3D modules. **a, b** Alizarin red S staining of bone nodules formed in the modules cultured for 21 days. Whole images (**a**), enlarged images under microscope (**b**), and quantitative analysis of mineralization (**c**) in the cultured modules. GFP, Dll1, or Dll4 represents GFP only, Dll1-, or Dll4-expressing MLO-Y4. *$p <$ 0.05 versus GFP group by one-way ANOVA, $n = 3$. Scale bar = 500 μm

towards osteoblasts. Surprisingly, we found that only osteocytic Dll4 could enhance the expression of Notch target genes Hes1, Hey1, and Hey2 in ST2 cells. However, osteocytic Dll1 and osteocytic Dll3 did not increase the expression of these Notch targets, and Hes1 expression was even decreased by Dll3 (Fig. 6d), suggesting that Dll4, but not Dll1 or Dll3, enhances Notch signaling compared to GFP control. Furthermore, the co-culture of MLO-Y4 cells, expressing individual Notch ligand, with ST2 cells was subjected to the Notch signaling inhibitor DAPT. Functionally, DAPT partially suppressed AP staining and reduced AP biochemical activity, indicating that the inhibition of Notch signaling decreases osteoblast differentiation (Figs. 6a and 6b). These results were further confirmed by the qPCR measurement, in which DAPT reversed the increased expression of osteoblast marker genes by osteocytic Dll4 to the control levels (Fig. 6c).

In order to further confirm such a mechanism, osteocytic Dll4 was used to induce osteoblast differentiation. Primary BMSCs were extracted from the femurs and tibiae of mice with a floxed functional exon of Notch signaling transcription factor RBPjκ (RBPjκ$^{f/f}$). The deletion of RBPjκ was successfully achieved by infection with adenovirus expressing Cre recombinase (Ad-Cre) that specifically recognizes and deletes the floxed exon of RBPjκ, resulting in a marked downregulation of the expression of Notch target genes Hey1, HeyL, and Hes7 (Figs. 7a and 7b). Notch signaling was disrupted in Ad-Cre infected RBPjκ$^{f/f}$ BMSCs compared to the Ad-GFP group. Moreover, Ad-Cre-infected RBPjκ$^{f/f}$ BMSCs showed a dramatic decrease in AP staining and the expression of osteoblast marker genes Alp, Runx2, and Osx, as compared to the Ad-GFP group (Figs. 7c and 7d).

When Ad-Cre-infected RBPjκ$^{f/f}$ BMSCs were co-cultured with MLO-Y4-Dll4 for 3 days, Notch signaling was completely shut down, as shown by notably decreased expression of Notch targets Hey1, HeyL, and Hes5 compared to the Ad-GFP group (Fig. 7e). Therefore, it was inferred that RBPjκ deletion in BMSCs eliminates their response to osteocytic Dll4, leading to the disruption of Notch signaling, similarly to the osteocytes overexpressing GFP (MLO-Y4-GFP). The Notch signaling-induced osteoblast differentiation was terminated, as shown by AP staining and the expression of osteoblast marker genes Alp, Runx2, and Osx in the co-culture of MLO-Y4-Dll4 with Ad-Cre infected RBPjκ$^{f/f}$ BMSCs when compared to the Ad-GFP group (Figs. 7f and 7g). No difference was detected in the levels of Notch signaling or osteoblast differentiation in RBPjκ$^{f/f}$ deleted

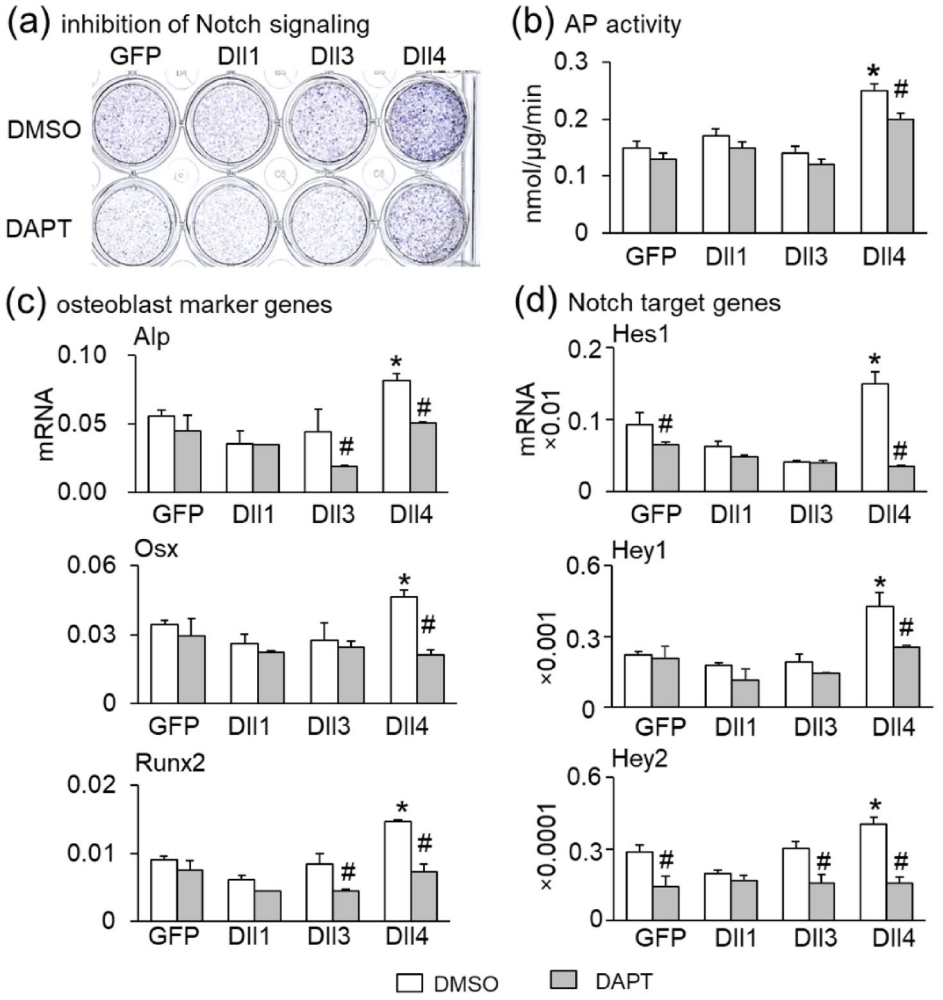

Fig. 6 Effect of Notch signaling on osteoblast differentiation in the co-cultures of osteocytes expressing Dll1, Dll3, or Dll4 with ST2 cells. **a–d** AP staining (**a**) and its biological activity assay (**b**); gene expression of osteoblast markers (**c**) and Notch targets (**d**) in the co-cultures. GFP, Dll1, or Dll4 represents GFP only, Dll1-, Dll3, or Dll4-expressing MLO-Y4. $^{*}p < 0.05$ versus GFP control; $^{\#}p < 0.05$ versus DMSO control by two-way ANOVA, $n = 3$

BMSCs co-cultured with MLO-Y4-Dll4 or MLP-Y4-GFP. Taken together, these findings indicated that Dll4 promotes osteoblast differentiation specifically by activating RBPjκ-dependent canonical Notch signaling.

Effect of osteocytic Dll4 on angiogenesis

Based on the coupling mechanisms between osteogenesis and angiogenesis, we detected the expression of angiogenesis marker genes in osteocytes overexpressing Dll4. We found that osteocytic Dll4 expressed a higher level of VEGFa and angiopoietin 1, which may lead to recruiting endothelial cells and inducing angiogenesis (Fig. 8a). To explore the role of Dll4 in osteocytes on angiogenesis, we used HUVECs co-cultured with MLO-Y4-Dll4 at a ratio of 1:4 in a 24-well plate pre-coated with Matrigel, and observed the formation of blood vessels for 6 h. We found increased vascular tubule formation in HUVECs cultured with MLO-Y4 cells compared to HUVECs cultured alone (Fig. 8b). The forming nodes and tubule lengths were increased by 292% and 151%, respectively, in the MLO-Y4-Dll4 group compared to HUVECs alone, and they were significantly higher (by 195% and 121%, respectively) than those in the MLO-Y4-GFP control (Fig. 8c). We further explored the angiogenic function of osteocytic Dll4 in 3D modules. The findings revealed that the expression of angiogenic marker genes Hif1α, eNOS and VE-Cad was higher than that in the GFP group when co-cultured with HUVEC for 3 days in the 3D modules (Fig. 8d). These results suggested that Dll4 in osteocytes enhances angiogenesis.

Discussion

In this study, we reconstructed a functional module by using a novel design of hard scaffolding material such as PCL integrated with cells by the so-called PCI3D technique. In this process, the nozzle temperature and cooling system of the platform may be adjusted to print hard materials firmly

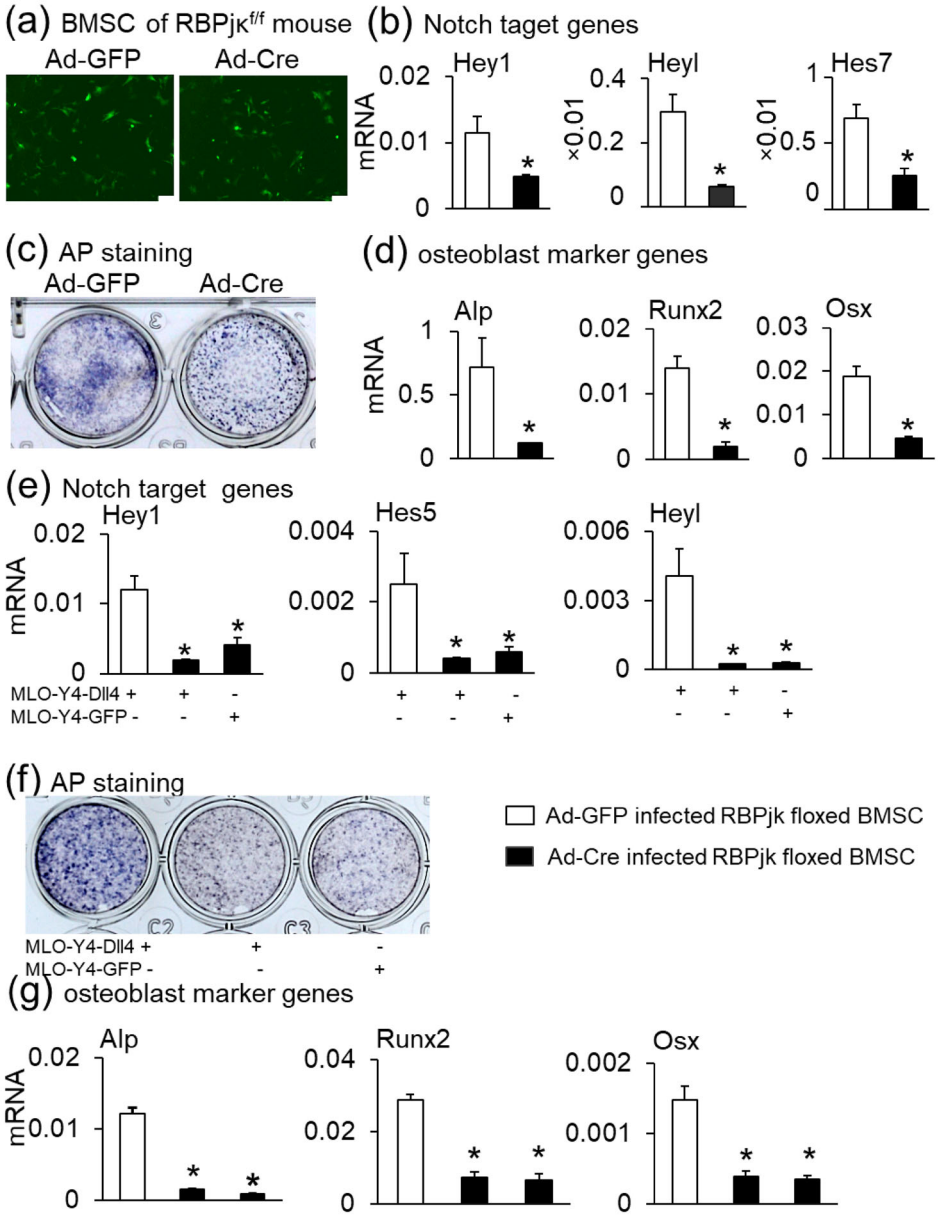

Fig. 7 Effect of canonical Notch signaling on osteoblast differentiation in the co-cultures of osteocytes expressing Dll1 or Dll4 with primary BMSCs. **a–d** Adenovirus-infected primary BMSCs from RBPjκ floxed mice infected with Ad-Cre. Images (**a**), gene expression of Notch targets (**b**), osteoblast differentiation assays by AP staining (**c**), and gene expression of osteoblast markers (**d**) of the BMSCs. *$p < 0.05$ versus Ad-GFP control by Student's t-test. $n = 3$. Scale bar = 100 μm. **e–g** Effects of canonical Notch signaling in RBPjκ-deleted primary BMSCs on the induction of osteoblast differentiation. **e** Gene expression of Notch targets; **f, g** osteoblast differentiation assays by AP staining (**f**) and gene expression of osteoblast markers (**g**). *$p < 0.05$ versus MLO-Y4-Dll4 + Ad-GFP-BMSC by one-way ANOVA, $n = 3$. Scale bar = 100 μm

and evenly until satisfying the requirement of concomitantly bio-printed cells for increased survival and growth. The cells provided an osteogenic microenvironment (osteocytic Dll4) for good cell viability (> 87%) and exhibited an about sixfold increase in proliferation in 7-day cultures. We found that osteocytic Dll4 induces osteoblast differentiation in both primary cells and a cell line of murine BMSCs in a co-cultured 2D system and in the PCI3D modules, which are good for mineralization. We identified that osteocytic Dll4 forms an independent active osteogenic microenvironment for BTE. Mechanistically, we demonstrated that osteocytic Dll4 promotes osteogenic differentiation by activating the RBPjκ-dependent canonical Notch signaling, and that osteocytic Dll4 also promotes angiogenesis. Therefore, the integration of cellular events into our novel PCI3D design has shed light on its ability to reconstruct bone integrity using osteocytic Dll4 for BTE.

Printing hard biomaterials together with cells into a scaffold is a huge challenge, especially in a structure supporting cell growth and specific functions. The current approach is to print 3D scaffolds of hard materials in advance, and seed cells on these scaffolds later. Although the cells can grow and differentiate towards osteoblasts on such 3D scaffolds, they can only enter the scaffold to a depth of 1 mm, beyond which few cells will grow. In the design of PCI3D, we assembled a material nozzle with a heating unit to melt PCL at 100 °C,

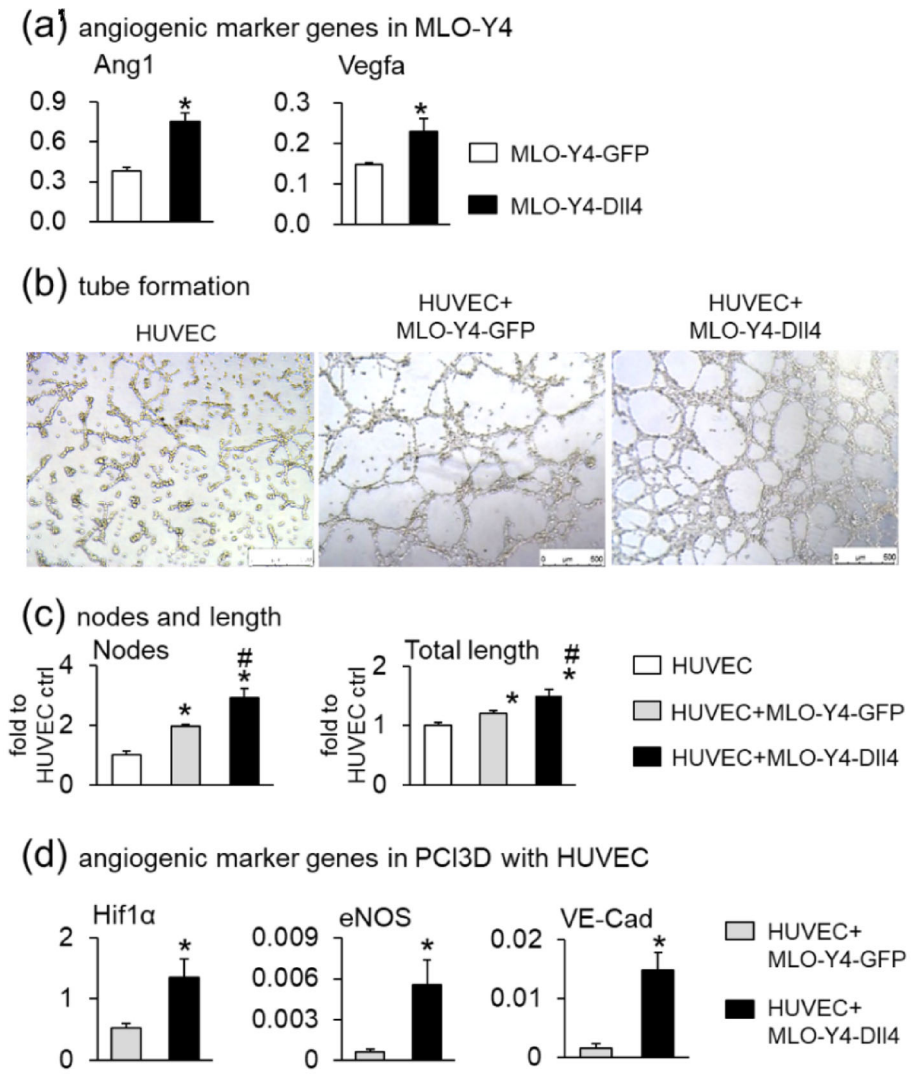

Fig. 8 Effect of osteocytic Dll4 on angiogenesis. **a** Angiogenic markers in MLO-Y4. **b** Images of vascular tubules forming in HUVECs upon co-culturing with MLO-Y4-Dll4 for 6 h. **c** Calculation of formed nodes (left) or tubule lengths (right). **d** Angiogenic markers in 3D co-culture system of HUVEC and MLO-Y4. $^{*}p < 0.05$ versus HUVEC control; $^{\#}p < 0.05$ versus MLO-Y4-GFP by one-way ANOVA, respectively, $n = 3$. Scale bar = 100 μm

and equipped it with a screw propeller to squeeze the melted PCL out of the nozzle as PCL beams at 95 °C, which made PCL beams lay down smoothly and evenly on the cooling platform. Meanwhile, bio-inks are commonly used to support cells to proliferate and play the role of growth factors [31]. We used blue light-curable GelMA hydrogel providing mechanical support for cell adhesion and proliferation as previously reported [12]. Besides, we identified an osteogenic factor that induces cell differentiation and mineralization, greatly enhancing BMSC function in the PCI3D modules. The novel design of PCI3D with the independent osteogenic factor would provide the Food and Drug Administration-approved hard scaffold material PCL with a biological environment suitable for morphogenesis, in order to obtain bone integrity for BTE.

Metabolic and functional bone artifacts may be fabricated by mimicking morphogenesis to an extent, in which the key developmental signaling pathways are needed to accelerate tissue formation in vitro [32]. Although we currently have a certain level of understanding of the Notch signal in physiological development process, the application of Notch signaling and its related components into tissue engineering is still very limited [33]. Integrating Notch signaling into tissue engineering can not only guide cell specific responses but also improve tissue engineering technology [34]. Research has shown that Jag1 construction directly immobilized on a novel poly (β-aminoester) transiently activated Notch signaling and increased osteogenesis [35]. In another study, the activation of Notch signaling on the surface of titanium implants improved its osteogenic properties [36]. Therefore, the activation of the Notch signaling pathway after injury has therapeutic potential for promoting bone formation in BTE.

Previously, scholars demonstrated that soluble Notch ligands cannot activate Notch signaling since it is hypersecreted

in nature [37–39]. In tissue engineering, for an effective signaling transduction between cells, the ligand must be anchored on the surface of the signal-sending cells and then bind to the receptor on the surface of the signal-receiving cells. In other words, the transduction through cell-to-cell contact ensures normal physiological function [40–45]. Therefore, it is necessary to achieve cell–cell communication and effective ligand–receptor pairs for the successful application of Notch signaling in tissue engineering. Our novel printing mode of bridging the contact between cells could transmit the activated Notch signaling pathway through the transcription factor RBPjκ, which was activated by overexpressing Dll4 in osteocytes, and then bound to more receptors on the surface of ST2 or BMSC. Any interference of this signal transduction would affect osteoblast differentiation.

Interestingly, our exploration of the vascular function on osteocyte Dll4 yielded unexpected results. While some studies have described the inhibitory effect of Notch ligand Dll4 in endothelial cells against angiogenesis [46–48], our research has indeed established that it has the function of promoting HUVEC cells to form tubules possibly due to the signal sending cells, i.e., the osteocytes. However, the specific mechanism awaits further investigations.

Cell therapy that combines signal cues with biomaterials is a complex process. Particularly, different from other signaling pathways, Notch signaling relies on the interaction of receptors and ligands to activate, which may be inhibited by any imbalance [49, 50]. In our study, we overexpressed the Notch signal ligand in bone cells through lentiviral transfection, activated the Notch signal in co-cultured BMSC or ST2, and promoted its osteogenic differentiation. However, we did not accurately control the signal dose. To this end, further research is needed to control the signal activation level accurately through Notch signal peptides from the biological material itself.

Conclusions

Our novel design of hard scaffolding material such as PCL and cell-integrated 3D printing system provides BMSCs with a stable structure and a biological microenvironment suitable for cells to grow and proliferate on PCL scaffolds. Osteocytic Dll4 acts as an independent active osteogenic microenvironment for BMSCs targeting the RBPjκ-dependent canonical Notch signaling pathway, with the unexpected function of angiogenesis. Tissue engineering with FDA-approved PCL 3D scaffolding in conjunction with Notch signaling events could be suitable for osteogenesis in vitro. Our results provide a basis for the development of tissue engineering by the integration of hard scaffolding material with a cellular event.

Acknowledgements The authors thank Professor Dr. Linda Bonewald for her kindly providing the MLO-Y4 cell line and appreciate Dr. Jun Li for his statistical analysis of data. This work is supported by the National Natural Science Foundation of China (Nos. U1601220, 82072450, and 81672118), Chongqing Science and Technology Commission-Basic Science and Frontier Technology Key Project (No. cstc2015jcyjBX0119), and Chongqing Medical University Intelligent Medicine Research Project (No.ZHYX202115).

Author contributions XLT, PTW, and ZSX contributed to conceptualization; XLT, XFW, and JC provided methodology; PTW, XFW, BW, and ZSX performed investigation; PTW, BW, and XL carried out data analysis; PTW and XL performed writing—original draft; all authors performed writing—review and editing; XLT contributed to funding acquisition; XLT provided resources; XLT and XL performed supervision.

Declarations

Conflict of interest The authors declare that they have no known competing financial interests or personal relationships that could have appeared to influence the work reported in this paper.

Ethical approval All animal procedures in our study were approved by the Institutional Animal Care and Use Committee of Chongqing Medical University.

References

1. Turnbull G, Clarke J, Picard F et al (2018) 3D bioactive composite scaffolds for bone tissue engineering. Bioact Mater 3(3):278–314. https://doi.org/10.1016/j.bioactmat.2017.10.001
2. Fan J, Lee CS, Kim S et al (2021) Trb3 controls mesenchymal stem cell lineage fate and enhances bone regeneration by scaffold-mediated local gene delivery. Biomaterials 264:120445. https://doi.org/10.1016/j.biomaterials.2020.120445
3. Amini AR, Laurencin CT, Nukavarapu SP (2012) Bone tissue engineering: recent advances and challenges. Crit Rev Biomed Eng 40(5):363–408. https://doi.org/10.1615/critrevbiomedeng.v40.i5.10
4. Borciani G, Montalbano G, Baldini N et al (2020) Co-culture systems of osteoblasts and osteoclasts: simulating in vitro bone remodeling in regenerative approaches. Acta Biomater 108:22–45. https://doi.org/10.1016/j.actbio.2020.03.043
5. Kang HW, Lee SJ, Ko IK et al (2016) A 3D bioprinting system to produce human-scale tissue constructs with structural integrity. Nat Biotechnol 34(3):312–319. https://doi.org/10.1038/nbt.3413
6. Malda J, Groll J (2016) A step towards clinical translation of biofabrication. Trends Biotechnol 34(5):356–357. https://doi.org/10.1016/j.tibtech.2016.03.003
7. Lieben L (2016) Regenerative medicine: the future of 3D printing of human tissues is taking shape. Nat Rev Rheumatol 12(4):191. https://doi.org/10.1038/nrrheum.2016.29
8. Murphy C, Kolan K, Li W, et al., (2017) 3D bioprinting of stem cells and polymer/bioactive glass composite scaffolds for bone tissue engineering. Int J Bioprint 3(1):53–63. https://doi.org/10.18063/IJB.2017.01.005
9. Piard C, Baker H, Kamalitdinov T et al (2019) Bioprinted osteon-like scaffolds enhance in vivo neovascularization. Biofabrication 11(2):025013. https://doi.org/10.1088/1758-5090/ab078a
10. Choudhury D, Tun HW, Wang T et al (2018) Organ-derived decellularized extracellular matrix: a game changer for bioink manufacturing? Trends Biotechnol 36(8):787–805. https://doi.org/10.1016/j.tibtech.2018.03.003

11. Swetha S, Lavanya K, Sruthi R et al (2020) An insight into cell-laden 3D-printed constructs for bone tissue engineering. J Mater Chem B 8(43):9836–9862. https://doi.org/10.1039/d0tb02019b
12. Hao Z, Song Z, Huang J et al (2017) The scaffold microenvironment for stem cell based bone tissue engineering. Biomater Sci 5(8):1382–1392. https://doi.org/10.1039/c7bm00146k
13. Liang X, Gao J, Xu W et al (2019) Structural mechanics of 3D-printed poly(lactic acid) scaffolds with tetragonal, hexagonal and wheel-like designs. Biofabrication 11(3):035009. https://doi.org/10.1088/1758-5090/ab0f59
14. Gao J, Ding X, Yu X et al (2021) Cell-free bilayered porous scaffolds for osteochondral regeneration fabricated by continuous 3D-printing using nascent physical hydrogel as ink. Adv Healthc Mater 10(3):e2001404. https://doi.org/10.1002/adhm.202001404
15. Confalonieri D, Schwab A, Walles H et al (2018) Advanced therapy medicinal products: a guide for bone marrow-derived MSC application in bone and cartilage tissue engineering. Tissue Eng Part B Rev 24(2):155–169. https://doi.org/10.1089/ten.TEB.2017.0305
16. Moreno Madrid AP, Vrech SM, Sanchez MA et al (2019) Advances in additive manufacturing for bone tissue engineering scaffolds. Mater Sci Eng C Mater Biol Appl 100:631–644. https://doi.org/10.1016/j.msec.2019.03.037
17. Rohban R, Pieber TR (2017) Mesenchymal stem and progenitor cells in regeneration: tissue specificity and regenerative potential. Stem Cells Int 2017:5173732. https://doi.org/10.1155/2017/5173732
18. Gigante A, Manzotti S, Bevilacqua C et al (2008) Adult mesenchymal stem cells for bone and cartilage engineering: effect of scaffold materials. Eur J Histochem 52(3):169–174. https://doi.org/10.4081/1208
19. Niedzwiedzki T, Filipowska J (2015) Bone remodeling in the context of cellular and systemic regulation: the role of osteocytes and the nervous system. J Mol Endocrinol 55(2):R23–R36. https://doi.org/10.1530/JME-15-0067
20. Robling AG, Bonewald LF (2020) The osteocyte: new insights. Annu Rev Physiol 82:485–506. https://doi.org/10.1146/annurev-physiol-021119-034332
21. Tu X, Delgado-Calle J, Condon KW et al (2015) Osteocytes mediate the anabolic actions of canonical Wnt/beta-catenin signaling in bone. Proc Natl Acad Sci USA 112(5):E478–E486. https://doi.org/10.1073/pnas.1409857112
22. Bai S, Kopan R, Zou W et al (2008) NOTCH1 regulates osteoclastogenesis directly in osteoclast precursors and indirectly via osteoblast lineage cells. J Biol Chem 283(10):6509–6518. https://doi.org/10.1074/jbc.M707000200
23. Engin F, Yao Z, Yang T et al (2008) Dimorphic effects of Notch signaling in bone homeostasis. Nat Med 14(3):299–305. https://doi.org/10.1038/nm1712
24. Hilton MJ, Tu X, Wu X et al (2008) Notch signaling maintains bone marrow mesenchymal progenitors by suppressing osteoblast differentiation. Nat Med 14(3):306–314. https://doi.org/10.1038/nm1716
25. Han H, Tanigaki K, Yamamoto N et al (2002) Inducible gene knockout of transcription factor recombination signal binding protein-J reveals its essential role in T versus B lineage decision. Int Immunol 14(6):637–645. https://doi.org/10.1093/intimm/dxf030
26. Tu X, Joeng KS, Nakayama KI et al (2007) Noncanonical Wnt signaling through G protein-linked PKCdelta activation promotes bone formation. Dev Cell 12(1):113–127. https://doi.org/10.1016/j.devcel.2006.11.003
27. Stern AR, Stern MM, Van Dyke ME et al (2012) Isolation and culture of primary osteocytes from the long bones of skeletally mature and aged mice. Biotechniques 52(6):361–373. https://doi.org/10.2144/0000113876
28. Billiet T, Gevaert E, De Schryver T et al (2014) The 3D printing of gelatin methacrylamide cell-laden tissue-engineered constructs with high cell viability. Biomaterials 35(1):49–62. https://doi.org/10.1016/j.biomaterials.2013.09.078
29. Venugopal JR, Giri Dev VR, Senthilram T et al (2011) Osteoblast mineralization with composite nanofibrous substrate for bone tissue regeneration. Cell Biol Int 35(1):73–80. https://doi.org/10.1042/CBI20090066
30. Zhang Q, Lu S, Li T et al (2019) ACE2 inhibits breast cancer angiogenesis via suppressing the VEGFa/VEGFR2/ERK pathway. J Exp Clin Cancer Res 38(1):173. https://doi.org/10.1186/s13046-019-1156-5
31. Daly AC, Freeman FE, Gonzalez-Fernandez T et al (2017) 3D Bioprinting for cartilage and osteochondral tissue engineering. Adv Healthc Mater 6(22):1700298. https://doi.org/10.1002/adhm.201700298
32. Majidinia M, Sadeghpour A, Yousefi B (2018) The roles of signaling pathways in bone repair and regeneration. J Cell Physiol 233(4):2937–2948. https://doi.org/10.1002/jcp.26042
33. Zohorsky K, Mequanint K (2021) Designing biomaterials to modulate Notch signaling in tissue engineering and regenerative medicine. Tissue Eng Part B Rev 27(5):383–410. https://doi.org/10.1089/ten.TEB.2020.0182
34. Rao SH, Harini B, Shadamarshan RPK et al (2018) Natural and synthetic polymers/bioceramics/bioactive compounds-mediated cell signalling in bone tissue engineering. Int J Biol Macromol 110:88–96. https://doi.org/10.1016/j.ijbiomac.2017.09.029
35. Dishowitz MI, Zhu F, Sundararaghavan HG et al (2014) Jagged1 immobilization to an osteoconductive polymer activates the Notch signaling pathway and induces osteogenesis. J Biomed Mater Res A 102(5):1558–1567. https://doi.org/10.1002/jbm.a.34825
36. Chakravorty N, Hamlet S, Jaiprakash A et al (2014) Pro-osteogenic topographical cues promote early activation of osteoprogenitor differentiation via enhanced TGFbeta, Wnt, and Notch signaling. Clin Oral Implants Res 25(4):475–486. https://doi.org/10.1111/clr.12178
37. Xia Y, Bhattacharyya A, Roszell EE et al (2012) The role of endothelial cell-bound Jagged1 in Notch3-induced human coronary artery smooth muscle cell differentiation. Biomaterials 33(8):2462–2472. https://doi.org/10.1016/j.biomaterials.2011.12.001
38. Urs S, Turner B, Tang Y et al (2012) Effect of soluble Jagged1-mediated inhibition of Notch signaling on proliferation and differentiation of an adipocyte progenitor cell model. Adipocyte 1(1):46–57. https://doi.org/10.4161/adip.19186
39. Vas V, Szilagyi L, Paloczi K et al (2004) Soluble Jagged-1 is able to inhibit the function of its multivalent form to induce hematopoietic stem cell self-renewal in a surrogate in vitro assay. J Leukoc Biol 75(4):714–720. https://doi.org/10.1189/jlb.1003462
40. Singh AB, Harris RC (2005) Autocrine, paracrine and juxtacrine signaling by EGFR ligands. Cell Signal 17(10):1183–1193. https://doi.org/10.1016/j.cellsig.2005.03.026
41. Chou CH, Modo M (2016) Human neural stem cell-induced endothelial morphogenesis requires autocrine/paracrine and juxtacrine signaling. Sci Rep 6:29029. https://doi.org/10.1038/srep29029
42. Yaron T, Cordova Y, Sprinzak D (2014) Juxtacrine signaling is inherently noisy. Biophys J 107(10):2417–2424. https://doi.org/10.1016/j.bpj.2014.10.006
43. Tang J, Peng R, Ding J (2010) The regulation of stem cell differentiation by cell-cell contact on micropatterned material surfaces. Biomaterials 31(9):2470–2476. https://doi.org/10.1016/j.biomaterials.2009.12.006
44. Peng R, Yao X, Cao B et al (2012) The effect of culture conditions on the adipogenic and osteogenic inductions of mesenchymal stem

cells on micropatterned surfaces. Biomaterials 33(26):6008–6019. https://doi.org/10.1016/j.biomaterials.2012.05.010
45. Cao B, Li Z, Peng R et al (2015) Effects of cell-cell contact and oxygen tension on chondrogenic differentiation of stem cells. Biomaterials 64:21–32. https://doi.org/10.1016/j.biomaterials.2015.06.018
46. Yang JM, Park CS, Kim SH et al (2020) Dll4 suppresses transcytosis for arterial blood-retinal barrier homeostasis. Circ Res 126(6):767–783. https://doi.org/10.1161/CIRCRESAHA.119.316476
47. Pitulescu ME, Schmidt I, Giaimo BD et al (2017) Dll4 and Notch signalling couples sprouting angiogenesis and artery formation. Nat Cell Biol 19(8):915–927. https://doi.org/10.1038/ncb3555
48. Benedito R, Roca C, Sorensen I et al (2009) The notch ligands Dll4 and Jagged1 have opposing effects on angiogenesis. Cell 137(6):1124–1135. https://doi.org/10.1016/j.cell.2009.03.025
49. Guruharsha KG, Kankel MW, Artavanis-Tsakonas S (2012) The Notch signalling system: recent insights into the complexity of a conserved pathway. Nat Rev Genet 13(9):654–666. https://doi.org/10.1038/nrg3272
50. Nandagopal N, Santat LA, LeBon L, et al., (2018) Dynamic ligand discrimination in the Notch signaling pathway. Cell 172(4):869–880 e19. https://doi.org/10.1016/j.cell.2018.01.002